Supporting Information

Xie et al. 10.1073/pnas.1011953108

SI Results and Discussion

Amplification of a Flicking Angle and Flagellum Realignment. Below we provide a calculation of the flicking angle amplified by the thrust force of the flagellar motor. It is shown that while in free swimming, the thrust force generated by the flagellum is sufficient to rotate the cell body by the observed amount ($\theta \sim 90°$). Moreover, a simple calculation using a resistive-force theory (RFT) indicates that the torque required for the realignment of the flagellum is $\sim 10^4$ pN·nm, which is of the same order of magnitude as the measured stalling torque of the flagellar motor (1). The calculation thus suggests that the flagellar motor is capable for flicking as well as for propulsion in cells of *Vibrio alginolyticus*.

For simplicity, we assume that the cell body rotates around its center of mass. The equation of motion for the cell-body rotation is given by

$$\gamma_1 \frac{d\theta}{dt} = bF \sin\theta, \qquad \text{[S1]}$$

where $\gamma_1 (\approx \frac{8\pi\eta b^3}{3(\ln(2b/a)-0.5)})$ is the rotational drag coefficient of the cell body (2), b is one-half the body length and is also the lever arm, a is the semiminor axis of the cell body, η is the dynamic viscous coefficient taken to be 10^{-3} N·s/m^2 as for water at 20°, $F = A_0 v_{sw}$ is the thrust generated by the flagellar motor, and $A_0 \approx 4\pi\eta b/(\ln(2b/a) - 0.5)$ is the linear drag coefficient of the body (2). This equation can be integrated with the result

$$\theta(t) = \cos^{-1}\left(\frac{C_0 \exp(-t/\tau) - 1}{C_0 \exp(-t/\tau) + 1}\right), \qquad \text{[S2]}$$

where $\tau = \gamma_1/2bF$, and $C_0 = (1 + \cos\theta_0)/(1 - \cos\theta_0)$ is determined by the initial bending angle θ_0. One can evaluate the time t for θ to reach 90°. This time is plotted versus θ_0 in Fig. S1, where, according to the values listed in Table S1, $\gamma_1 = 0.29 \times 10^{-19}$ N·m·s and $F = 0.67 \times 10^{-12}$ N were used. It is seen that t increases rapidly as θ_0 decreases. For $\theta_0 = 10°$, $t = 0.06$ s, which is about two video frames and is consistent with our observation in Fig. 4 *A–E*. However, in some of our video images, initial angles as large as 40° were observed, suggesting that the initiation of flicking may not be totally passive, and in this case rotating by 90° takes less than 0.03 s. We found that the above calculation does not strongly depend on the assumption about the location of the rotation axis. For instance, by assuming that the cell rotates about a fixed axis at the front end of the cell body, t only changes by about 15% and thus will not significantly alter our above conclusion.

It is remarkable that after flicking, the flagellum realigns itself swiftly with the cell-body axis, and the bacterium resumes its forward swimming. Although it is unclear how this last step is accomplished at a molecular level, we wish to know if the torque involved is within the limit of the flagellar motor of *V. alginolyticus*. As depicted in Fig. 4*F*, the motion of the flagellum at this step is rather complex. It involves the whole flagellum swinging about the cell-body axis with the tip of the flagellum tracing out a hyperbolic spiral. The sweeping angular frequency ω_R based on our fluorescence microscopic measurements is $\omega_R/2\pi \approx 30$ Hz. A full hydrodynamic calculation of the torque is difficult, and in the following we seek a simpler calculation using the RFT (3).

We assume that in the lab coordinates (x, y, z) the cell body is along the z axis, and the flagellum rotates about the x axis with a constant angular velocity ω_R. At the end of rotation it aligns with the body axis as depicted in Fig. S2. We assign a fixed local coordinate (x', y', z') on the flagellum, and within this coordinate system the flagellum can be parameterized as

$$\vec{h}(s) = (R\cos ks, R\sin ks, \sqrt{1 - k^2R^2}s), \qquad \text{[S3]}$$

where R is the radius of the helix, k is the wavenumber measured along the contour, and s is the contour length along the flagellum. Without losing generality, let x' axis be parallel to the rotation axis x at all times and z' axis coincide with y axis at $t = 0$ as depicted in Fig. S2. We will calculate the torque based on this instantaneous configuration, but the result holds for other angular positions of the flagellum. Assuming for simplicity that the flagellum does not rotate about its own symmetry axis z', the velocity of the flagellar segment located at s to $s + ds$ in the local coordinates can be readily calculated as

$$\vec{v}(s) = \vec{\Omega} \times \vec{h}(s) = (0, -\sqrt{1 - k^2R^2}\omega_R s, \omega_R R\sin ks), \qquad \text{[S4]}$$

where $\vec{\Omega} = (\omega_R, 0, 0)$ is the angular velocity. This velocity can be decomposed into the tangential component $\vec{v}_t$ and the normal component $\vec{v}_n$ with the result,

$$\begin{aligned}\vec{v}_t(s) &= (\vec{v}(s) \cdot \hat{t}(s))\hat{t}(s) \\ &= \sqrt{1 - k^2R^2}\omega_R R(-ks\cos ks \\ &\quad + \sin ks)(-Rk\sin ks, Rk\cos ks, \sqrt{1 - k^2R^2}), \end{aligned} \qquad \text{[S5]}$$

$$\vec{v}_n(s) = \vec{v}(s) - \vec{v}_t(s), \qquad \text{[S6]}$$

where $\hat{t}(s) = (-Rk\sin ks, Rk\cos ks, \sqrt{1 - k^2R^2})$ is a unit vector along the tangential direction of the flagellum. The tangential and the normal force on the segment can be obtained from Eqs. **S5** and **S6**:

$$\vec{F}_t(s)ds = K_t\vec{v}_t(s)ds, \qquad \text{[S7]}$$

$$\vec{F}_n(s)ds = K_n\vec{v}_n(s)ds, \qquad \text{[S8]}$$

where $K_t = \frac{2\pi\eta}{\ln(2\Lambda/r)-1/2}$ and $K_n = 2K_t$ are, respectively, the tangential and the normal viscous coefficient. In the above, r is the radius of the flagellar filament and Λ is the pitch. The net force per unit length is given by $\vec{F}(s) = \vec{F}_t(s) + \vec{F}_n(s)$ and the torque per unit length about the rotation axis x is then given by $d\vec{N}_R = \vec{h}(s) \times \vec{F}(s)$. The total torque on the flagellum is obtained by integrating s from 0 to L,

$$\vec{N}_R = \int_0^L \vec{h}(s) \times \vec{F}(s)ds. \qquad \text{[S9]}$$

The result of this integral consists of terms proportional to L^3 and $O(L^2)$ terms. It is clear that the $O(L^2)$ terms are due to fringe fields, and for a long helix the leading term is

$$\vec{N}_R = \left(\frac{1}{3}K_n L^3\beta\left[1 - \frac{1}{2}(1-\beta)(1-\gamma_k)\right]\omega_R, 0, 0\right), \qquad \text{[S10]}$$

where $\beta = \cos^2 \Psi = 1 - R^2k^2$ with Ψ being the pitch angle and $\gamma_k = K_t/K_n = 1/2$.

Using the measured geometric parameters tabulated in Table S1, we found $N_R \approx 10^4$ pN·nm. This value is about three times greater than the stalling torque, $N_{\max} = 3 \times 10^3$ pN·nm, measured by Sowa et al. (1). Considering the approximation made about the movement of the flagellum in the calculation, the discrepancy between the measurement and the calculation may not be considered significant. Hence, it is likely that the flagellar motor alone may be sufficient in powering the sweeping motion seen in the experiment. However, it remains a possibility that a part of the energy driving the flicking motion may be stored as elastic energy in the motor-flagellar complex when the flagellum is off axis with respect to the cell body. The sweeping motion of the flagellum then may be interpreted as an instability that allows the stored elastic deformation to be released, causing the flagellum to realign with the cell-body axis. We would like to emphasize that presently nothing is known about the molecular components that are responsible for the flicking movement. Our calculation simply shows that the energy or the torque required is compatible with what we know about the flagellar motor. The calculation certainly cannot rule out the possibility that this important process is driven by another independent power source.

Time-Difference Probability Density Functions in a Homogeneous Medium. In a homogeneous medium without chemoeffectors, the distributions of the time intervals t_f and t_b in *V. alginolyticus* were found in Fig. 3 *B* and *C* to peak at a short time of ~0.2 and ~0.3 s, respectively. This indicates that the regulation of the motor-rotation intervals is not a Poisson process, differing from that of *Escherichia coli* (4). Interestingly, however, we found that the difference in the time intervals $t_f - t_b$ is distributed in a Poissonian fashion, which is displayed in Fig. S3*A*. For clarity, we also plotted the same data in the *Insets* for $t_f - t_b > 0$ and $t_f - t_b < 0$, separately. It is clear that the probability density function (PDF) $P(t_f - t_b)$ is approximately symmetric with respect to $t_f - t_b = 0$, raising the question of whether the chemotaxis network of *V. alginolyticus* differentiates forward from backward swimming in a steady state. Fitting the experimental data with exponential functions, we found two characteristic times 0.29 s and 0.34 s for $t_f - t_b < 0$ and $t_f - t_b > 0$, respectively. For convenience, we also plot $P(|t_f - t_b|)$, which is displayed in Fig. S3*B*. Because the characteristic times for $t_f - t_b > 0$ and $t_f - t_b < 0$ are reasonably close, $P(|t_f - t_b|)$ is also approximately exponential as expected.

Because of the time reversal symmetry between the forward and backward swimming within each three-step cycle, the net displacement of the bacterium per cycle is $l = v_{sw}|t_f - t_b|$, where v_{sw} is the swimming speed of the bacterium. Furthermore, because the flick reorients the cell body stochastically with the highest probability at $\theta \sim 90°$, the displacements between cycles are uncorrelated. Hence, the swimming trajectories of *V. alginolyticus* resemble a random walk with Poisson steps l in the steady state.

Three-Step Strategy near a Sharp Chemical Gradient. To understand how *V. alginolyticus* perform chemotaxis, we carried out a tracking experiment near a micropipette tip filled with 1 mM serine. Pairs of (t_f, t_b) were measured and plotted in Fig. 3*D*. In contrast with Fig. 3*A*, where t_f and t_b are uncorrelated in the absence of chemoeffectors, strong correlations emerge between t_f and t_b when a sharp gradient is present. One of the branches features $t_f \sim t_b$ with a proportionality constant of 0.86 as delineated by the solid line in Fig. 3*D*. This constant, which deviates slightly from unity, may be attributed to a small bias in the swimming speeds; i.e., for *V. alginolyticus* the backward swimming speed v_b was found to be ~10% higher than the forward speed v_f. Thus, the forward and backward displacements in a cycle are about the same, $v_f t_f \sim v_b t_b$, leading to a small net displacement l. The other branch, where t_f is much smaller than t_b, corresponds to a "correction" response, which will be discussed below.

It has been shown that there is a drastic change in $P(t_f)$ and $P(t_b)$ when a sharp chemical gradient is present (see Fig. 3 *B*, *C*, *E*, and *F*). A correspondingly large change is also observed in $P(t_f - t_b)$, as displayed in Fig. S4. Unlike in Fig. S3*A*, one observes that the PDF is strongly skewed (~30%) toward the negative side. It is composed of two peaks: One is centered around zero, corresponding to the $t_f \sim t_b$ branch in Fig. 3*D*, and the other is centered around $t_f - t_b \approx -1$ s, corresponding to the branch with small t_f but large t_b in Fig. 3*D*. The two groups of data resulted from different orientations of the cell body after a flick; e.g., when the flick directs the cell toward the source, t_f and t_b will be correlated (or $t_f \sim t_b$), but when the flick directs the cell away from the source, t_f and t_b will be anticorrelated (i.e, a short forward is followed by a long backward movement).

The above peculiar correlations between t_f and t_b can be best illustrated by the simple physical picture depicted in Fig. S5*A*, which is supported by the measured trajectories in Fig. S5*B*. Imagine that a bacterium traverses a region of radius R containing attractant, and the region outside R is devoid of attractant. Suppose initially the bacterium swims backward, and at the edge of the boundary, the cell flicks and randomly picks a new direction as depicted by 1–2 or 1*–2* segments in the figure. For a sufficiently large radius R, ~50% of the flicking events will reorient the cell to outside R and the subsequent forward swimming interval (or the distance) will be short, which is indicated by segment 3 in the figure. This contributes to the sharp peak in $P(t_f)$ in Fig. 3*E*. On the other hand, the other 50% of the flicking events will reorient the cell to point inside R, as depicted by segment 3* in the figure. The cell swims forward for a long distance until it reaches the boundary on the other side, it then backtracks over the same distance, and it flicks again at the boundary. In this case, the backward swimming interval (segment 4*) is strongly correlated with the forward interval (segment 3*). Because the flicking angle is random, different lengths are generated inside R, as illustrated in Fig. S5*B*. This yields a broad distribution in both $P(t_f)$ and $P(t_b)$ and gives rise to the strong correlation between pairs of t_f and t_b seen in the experiment.

Swarming Around a Point Source of Chemoattractant. We also investigated how the swarming behavior is affected by the serine concentration c_0 in the micropipette (see *SI Materials and Methods*). Here, we only focus on the steady-state bacterial distributions. Fig. S6*A* displays $r_{1/2}$ for *E. coli* (circles) and *V. alginolyticus* (squares). The dotted line in the figure denotes the radius σ for the serine profile $c(r)$. We found that $r_{1/2}$ for *V. alginolyticus* is very weakly dependent on c_0; i.e. varying c_0 by three orders of magnitude, $r_{1/2}$ changes by only about a factor of two. Our data also suggest that there exists a minimum in $r_{1/2}$, which occurs in the neighborhood of 1 mM. Likewise, $r_{1/2}$ also changes little for *E. coli*. As shown in Fig. S6*A*, a two-order-of-magnitude change in serine (0.5–50 mM) resulted in a twofold change in $r_{1/2}$ (125 to 265 μm), which is reminiscent of the additive rule in *E. coli* adaption (5, 6). Unfortunately, we were unable to measure $r_{1/2}$ for $c_0 < 0.5$ mM in *E. coli* because the bacterial profile was too flat to be measured reliably. Fig. S6*B* shows the contrast $I_{\max}/I_\infty$, which is a measure of $B_{\max}/B_\infty$, as a function of c_0. One observes that for both bacterial species, this contrast factor decreases precipitously for $c_0 \leq 0.05$ mM, and this threshold of swarming is significantly higher than K_I, which for *E. coli* is 18 μM (7, 8). This suggests that the threshold of chemical detection K_I and the ability to swarm are not completely correlated; in other words, for cells to benefit from a narrowly distributed nutrient source, both the chemical sensitivity and the strategy of exploitation are essential. We noticed that our measured $I_{\max}/I_\infty$ vs. c_0 for *E. coli* is similar to that seen in the standard capillary assay where the number of bacteria entering the capillary for a fixed incubation time is

plotted against the chemoeffector concentration. For instance, the peak position ~5 mM found in ref. 9 is nearly identical to ours.

The ability for bacteria to stay close to a source is important for increasing their nutrient uptake and can be characterized by $C = \langle B(r)c(r)\rangle / (\langle B(r)\rangle\langle c(r)\rangle)$. The calculated C is presented in Fig. S6*C* for different serine concentrations. It is evident that for the given distribution $c(r)$, C for *V. alginolyticus* is much greater than that of *E. coli*, indicating that during competitive foraging, the former is more advantageous than the latter.

Swimming Trajectories of *Pseudoalteromonas haloplanktis*. In an earlier work exploring rapid chemotactic response of *P. haloplanktis*, it was reported that *P. haloplanktis* displayed a remarkable chemotactic advantage over *E. coli* (10). According to a computer model, the investigators concluded that the higher swimming speed increases the chemotactic advantage of *P. haloplanktis*, but to a smaller degree than observed in the experiments. They speculated that the bacteria rely on additional behavioral strategies, which was attributed to the run–reverse swimming pattern of *P. haloplanktis* (10). Because, similar to *V. alginolyticus*, *P. haloplanktis* have a single polar flagellum, we were curious about whether *P. haloplanktis* also adopt the three-step strategy. Because these bacteria swim at a higher speed and for a longer time before a reversal, tracking is more difficult as they easily get out of the field of view or become defocused. As a result, presently we do not have extensive statistics about how *P. haloplanktis* swim. However, based on our limited data, it is evident that *P. haloplanktis* incorporate flicks into their motility. Using the 40× objective, we can resolve their body orientations; it is commonly observed that the long axis of the cell body reorients by as much as 90° from one frame to the next within 1/30 s. Examining the motility pattern of *P. haloplanktis* carefully, we found that the bacterial trajectories also consist of intermediate angular changes similar to those flicking angles observed in *V. alginolyticus*. We also obtained several bacterial tracks (see Fig. S7) that seem to be three-step cycles, although we are unsure whether all cells exhibit the same pattern or whether the flick occurs during the transition from backward to forward swimming or vice versa. It remains an intriguing possibility that the flicking step in *P. haloplanktis* could be "on-demand"; namely, the cell flicks only when necessary. This would represent a more advanced chemotactic strategy than the cyclic three-step process we found in *V. alginolyticus*. It certainly would require more components and perhaps more sophisticated chemotactic regulation. This important issue can be clarified only when more controlled experiments are carried out. One thing that can be concluded from all these observations, however, is that backtracking and flicking are important for bacteria living in oceans where nutrients appear and disappear rapidly.

SI Materials and Methods.

Plasmids, Bacterial Strains, and Cultures. The plasmid pZA3R-YFP was a gift of Hanna Salman. It has a P15A replicon, confers a chloramphenicol resistance, and encodes YFP proteins. Both *V. alginolyticus* and *E. coli* were transformed with the plasmid following the procedure described in ref. 11.

For the growth of *V. alginolyticus*, we followed the protocols in ref. 1. Strains YM4 (with or without the pZA3R-YFP plasmid), VIO5, and 138-2 (12) were grown at 30 °C with vigorous shaking at 200 rpm overnight in VC medium (5 g polypeptone, 5 g yeast extract, 4 g K_2HPO_4, 30 g NaCl, 2 g glucose, 10^3 mL H_2O, supplemented with 2.5 μg/mL chloramphenicol when needed). The overnight was diluted 1 : 100 into VPG medium (10 g polypeptone, 4 g K_2HPO_4, 30 g NaCl, 5 g glycerol, 10^3 mL H_2O, supplemented with 2.5 μg/mL chloramphenicol when needed) and grown to late-exponential phase. Cells were spun down and resuspended in TMN motility medium [50 mM Tris-HCl (pH 7.5), 5 mM $MgCl_2$, 5 mM glucose, 30 mM NaCl, 270 mM KCl] and incubated for at least 30 min at 30 °C, while being shaken at 200 rpm.

E. coli RP437-YFP cells were grown overnight in M9 medium supplemented with 30 μg/mL chloramphenicol at 30 °C to reach an optical density of 0.2. The cells were then carefully washed and resuspended with motility buffer (10 mM potassium phosphate, 0.1 mM EDTA, 10 mM sodium-L-lactate, 1 μM L-methionine, pH 7.0).

P. haloplanktis were obtained from the American Type Culture Collection (ATCC 700530) and grown overnight in 1% tryptic soy broth at room temperature, shaking at 200 rpm. The culture was diluted 1 : 200 into filtered sea water and starved at room temperature for 5 h before observation (10).

Methods for Tracking and Swarming Experiments. A serine-filled micropipette was used to create a sharp attractant gradient in our experiment. The micropipette was prepared as described in *Materials and Methods* and filled with different concentrations of serine to a height that balanced the capillary effect. This tip was inserted into a micropipette adaptor (World Precision Instrument, 5430-15), and could be precisely positioned by a motorized 3D micromanipulator (SD instruments, MX7630L). The tip of the micropipette was adjusted to ~200–300 μm above the surface of the open observation chamber. A small pressure created by a water column provided a constant flux of attractant at the tip. To measure the injection rate, we placed the micropipette filled with 100 mM fluorescein in the chamber containing 400 μL motility buffer. A small volume of fluid in the chamber was sampled periodically after thorough mixing, and its fluorescence was measured by a fluorescent spectrometer (Perkin Elmer, LS-3B). This measurement yields an injection rate of 6×10^{-12} L/s. Thus, during our experiments, which typically lasted for less than 10^3 s, the background serine concentration at most rose to 1 μM, which is about 10 times less than the sensitivity of *E. coli* to serine.

Using the above setup, we also calibrated the dye distribution near the tip using the CCD camera (Hamamatsu, EM-CCD C9100-12), and video images were analyzed by SimplePCI (Compix Inc.). The background subtracted fluorescence intensity $I_c(r)$ was normalized and presented as the thick orange lines in Fig. 5 *A* and *B*. We found that at a large distance from the center, the intensity decays as $1/r$, and the radius at the half-height is $\sigma = 9.7$ μm. By stirring the surrounding medium, we also found that the dye profile can be established almost instantaneously, in less than 1 s, and it is stable over a long period of time, indicating a quasi steady state. Because the molecular diffusivities of serine and fluorescein are close, with $D = 9 \times 10^{-6}$ and 6×10^{-6} cm^2/s, respectively, the serine distribution $c(r)$ is assumed to follow the dye distribution characterized by $I_c(r)$.

To observe YM4's swimming patterns near the micropipette tip filled with $c_0 = 1$ mM serine, we first stirred up the fluid in the chamber to produce a uniform cell distribution. We then video recorded the chemotactic activities of the bacteria using the Hamamatsu camera under a 20× phase contrast objective. When the cell density was low, bacteria could be followed for the first 30 s near the tip, and statistics of pairs of consecutive swimming intervals (t_f, t_b) were collected over many trials. However, in long times, >1 min, the cell density near the tip became so large that tracking of individual cells became impossible. These long-time video clips allowed us to estimate the swarm size R, which we used in Fig. S5 *A* and *B*.

The above measurements were repeated for several concentrations of serine, $c_0 = 5 \times 10^{-4}, 5 \times 10^{-3}, 5 \times 10^{-2}, 0.5, 5$, and 50 mM, using both *V. alginolyticus* YM4-YFP and *E. coli* RP437-YFP. Instead of studying swimming patterns, here we focused on their swarming abilities near the point source. For both bacterial strains, noticeable aggregation occurred when $c_0 \geq 50$ μM. For *E. coli*, the swarm became so large when $c_0 > 50$ mM that it expanded beyond

the field of view of our camera. Thus, only in the concentration range, $5 \times 10^{-2} < c_0 < 50$ mM, we were able to generate data by which both bacteria could be compared. In the measurement, video recording started immediately after the sample was stirred and lasted for up to 12 min, depending on the swarming speed.

To minimize possible photodamage due to the excitation light ($\lambda = 488$ nm), a computer-controlled shutter was introduced between the arc lamp and the collimator of the epifluorescence attachment of the microscope. The shutter was interfaced via a data acquisition board (National Instruments, PCI-6601) and Labview (National Instruments). The shutter opened periodically at a fixed interval $T = 2$ or 3 s depending on the video speed [former for 10 frames per second (fps) and latter for 5 fps], and the shutter opening time was set at $T/10$. Thus, during the measurement, bacteria were only exposed to light 10% of the time.

For each serine concentration used, fluorescent intensity due to the fluorescent bacteria was measured. A uniform initial cell density 10^7 mL^{-1} was kept fixed in all runs. The time-dependent intensity was background subtracted and circularly averaged according to the procedure delineated in *Materials and Methods*. The normalized average intensity $I(r,t)$ and its steady-state value $I(r)$ are plotted in Fig. 5 *A* and *B* for both *V. alginolyticus* (*A*) and *E. coli* (*B*), where $I(r,t)$ and $I(r)$ are proportional to the bacterial concentrations $B(r,t)$ and $B(r)$. The measured intensity profiles $I(r,t)$ were spline fit so that radii $r_{1/2}$ at half maxima ($I(r_{1/2},t) = \max(I(r,t))/2$) as a function of time t and c_0 were calculated. The fitting procedure also allowed us to find the contrast factor $I_{\max}/I_\infty$, which is the ratio of the maximum intensity and the intensity when cells are uniformly distributed. This ratio is a measure of the cell density near the center of the swarm compared to that in the far field, $B_{\max}/B_\infty$. A tighter and denser swarm near the point source suggests a higher nutrient exposure, which can be qualitatively determined in our experiment by computing the correlation $\langle B(r)c(r)\rangle/(\langle B(r)\rangle\langle c(r)\rangle) \sim \langle I(r)I_c(r)\rangle/(\langle I(r)\rangle\langle I_c(r)\rangle)$, where $I_c(r)$ is the steady-state intensity of fluorescein, and the angle brackets are defined as $\langle f(r)\rangle = \int f(r)rdr/\int rdr$.

1. Sowa Y, Hotta H, Homma M, Ishijima A (2003) Torque-speed relationship of the Na^+-driven flagellar motor of *Vibrio alginolyticus*. *J Mol Biol* 327:1043–1051.
2. Berg HC (1993) *Random Walks in Biology* (Princeton Univ Press, Princeton).
3. Gray J, Hancock GJ (1955) The propulsion of sea-urchin spermatozoa. *J Exp Biol* 32:802–814.
4. Block SM, Segall JM, Berg HC (1983) Adaptation kinetics in bacterial chemotaxis. *J Bacteriol* 154:312–323.
5. Spudich JL, Koshland DE (1975) Quantitation of the sensory response in bacterial chemotaxis. *Proc Natl Acad Sci USA* 72:710–713.
6. Berg HC, Tedesco PM (1975) Transient response to chemotactic stimuli in *Escherichia coli*. *Proc Natl Acad Sci USA* 72:3235–3239.
7. Levit MN, Grebe TW, Stock JB (2002) Organization of the receptor-kinase signaling array that regulates *Escherichia coli* chemotaxis. *J Biol Chem* 277:36748–36754.
8. Mello B, Tu Y (2007) Effects of adaptation in maintaining high sensitivity over a wide range of backgrounds for *Escherichia coli* chemotaxis. *Biophys J* 92:2329–2337.
9. Mesibov R, Adler J (1972) Chemotaxis toward amino acids in *Escherichia coli*. *J Bacteriol* 112:315–326.
10. Stocker R, Seymour JR, Samadani A, Hunt DE, Polz MF (2008) Rapid chemotactic response enables marine bacteria to exploit ephemeral microscale nutrient patches. *Proc Natl Acad Sci USA* 105:4209–4214.
11. Kawagishi I, Okunishi I, Homma M, Imae Y (1994) Removal of the periplasmic DNase before electroporation enhances efficiency of transformation in the marine bacterium *Vibrio alginolyticus*. *Microbiology* 140:2355–2361.
12. Kojima S, et al. (1997) *Vibrio alginolyticus* mutants resistant to phenamil, a specific inhibitor of the sodium-driven flagellar motor. *J Mol Biol* 265:310–318.

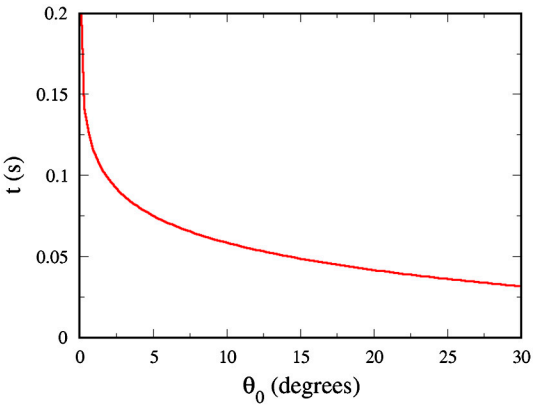

Fig. S1. The time t required for the cell body to rotate 90° as a function of the initial bending angle θ_0. The calculation shows that as long as $\theta_0 > 10°$, t depends weakly on θ_0 and is typically less than 0.05 s, which is consistent with our observations.

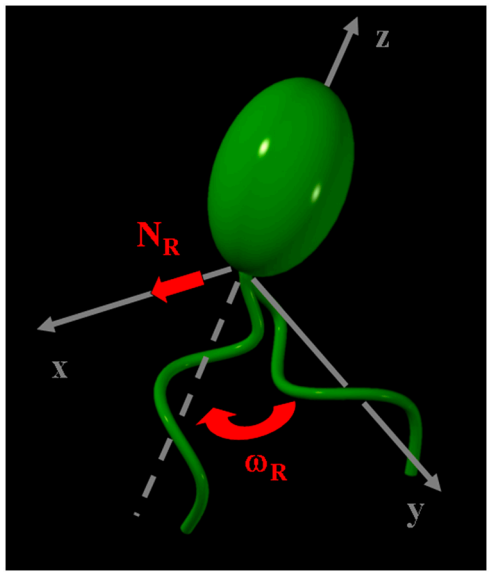

Fig. S2. A simplified flagellum movement at the end of the flicking process. In contrast to Fig. 4 *F*, here, in order to facilitate the calculation, we assume that the flagellum is initially along the *y* axis, and it rotates about the *x* axis until it aligns with the bacterial cell-body, or *z* axis. The rotational angular frequency is $\omega_R \approx 2\pi \times 30$ Hz, and the torque $N_R \approx 10^4$ pN·nm is calculated using the RFT.

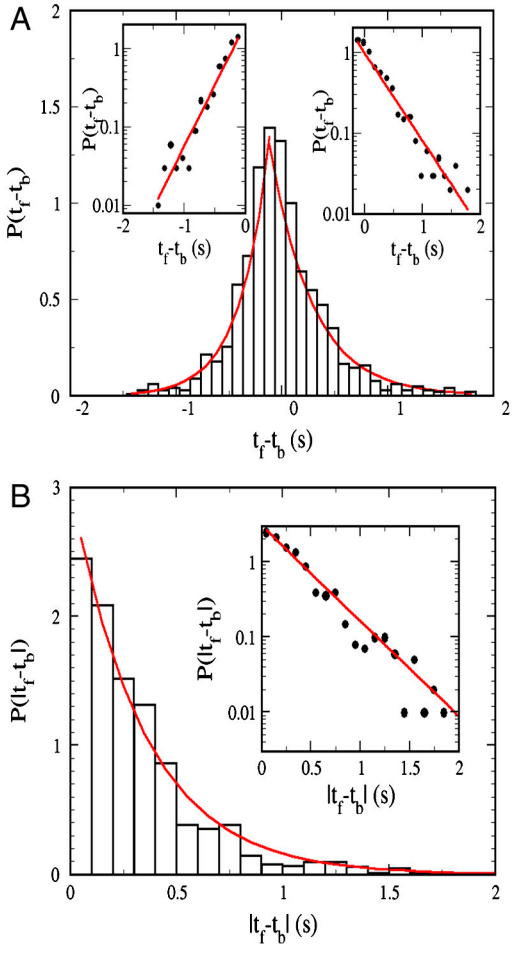

Fig. S3. The PDF $P(t_f - t_b)$ and $P(|t_f - t_b|)$ measured in TMN. It is seen in *A* that $P(t_f - t_b)$ is centered about zero with a small (~3%) skewness toward $t_f - t_b < 0$. The red lines are fits to exponential functions. The goodness of the fits is also displayed in the *Insets*, where the same data were replotted in a semilog fashion for $t_f - t_b > 0$ and $t_f - t_b < 0$, separately. The Poisson time in these two regimes are, respectively, 0.29 and 0.34 s. In *B*, it is shown that $|t_f - t_b|$ is also distributed approximately exponentially with a characteristic time of 0.31 s.

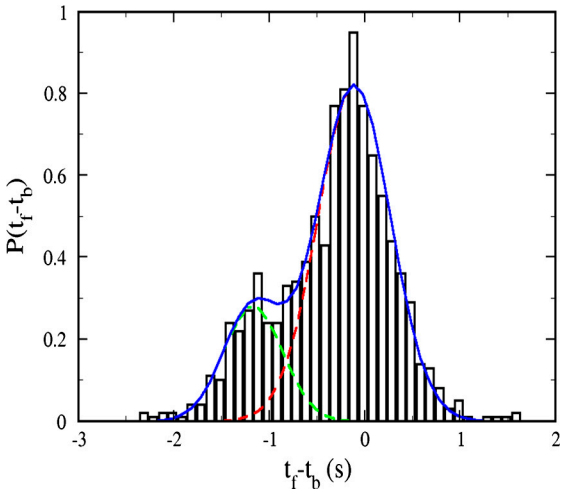

Fig. S4. The PDF $P(t_f - t_b)$ measured in a chemical gradient created by a point source of attractant (1 mM serine). Unlike in a homogeneous TMN (see Fig. S3), when a point source of attractant is present, $P(t_f - t_b)$ is no longer symmetric between $t_f - t_b > 0$ and $t_f - t_b < 0$, indicating strong correlations between forward and backward swimming. The distribution consists of two peaks, which we modeled using two Gaussian functions and plotted as red and green dashed lines. The sum of the two was plotted as the blue solid line, which mimics our measured PDF well. Physically, the dominant peak is contributed by events when $t_f \approx t_b$, and the minor peak is due to events when $t_f \ll t_b$. See *SI Results and Discussion* for more details.

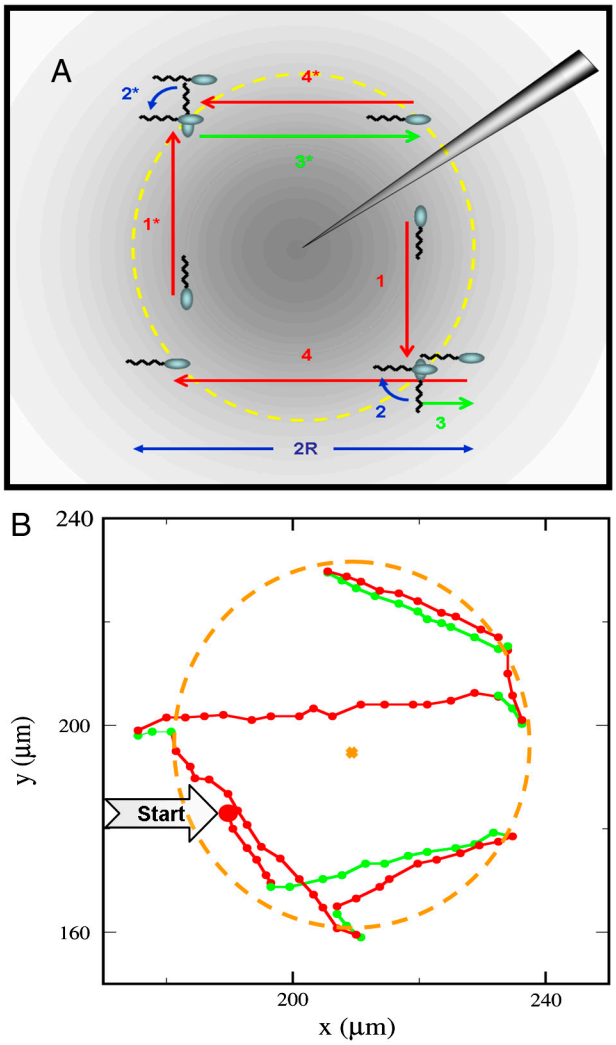

Fig. S5. Bacterial chemotactic behaviors in a chemical gradient created by a micropipette tip filled with attractant. (*A*) Localization of bacteria near a sharp chemical gradient. A serine-filled micropipette tip introduces a quasi-stationary concentration gradient in a liquid medium. The bacterium carries out chemotaxis as described in *SI Results and Discussion*. Near the point source of attractant, there are two different scenarios depicted at the *Upper Left* corner and the *Lower Rright* corner. Here, t_f and t_b are correlated for the *Upper Left* trajectories, but "anticorrelated" in the *Lower Rright* trajectories; i.e. a short forward swimming segment is most likely to be accompanied by a long backward swimming segment. (*B*) A measured *V. alginolyticus* trajectory near a micropipette tip. The cross at the center is the location of the pipette tip filled with 1 mM serine, and the circle (dashed line) is approximately the outer edge of the swarm. The large solid circle is the starting position of the bacterial track, which consists of forward (green) and backward (red) swimming segments. The small dots represent the positions of the bacterium at an equal time interval of 0.067 s.

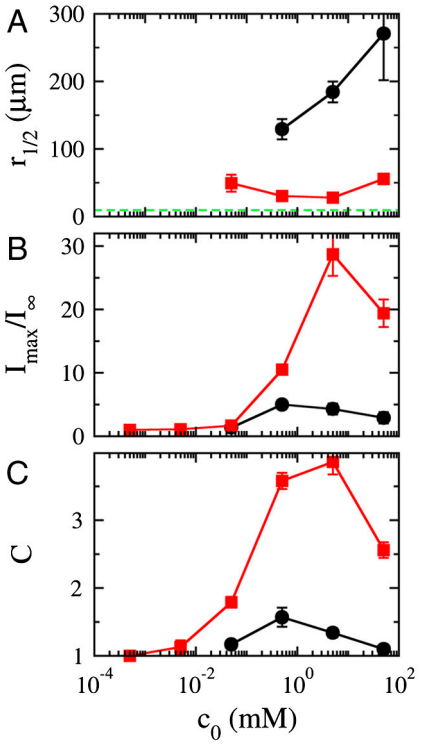

Fig. S6. Swarming behavior as a function of serine concentration c_0. The data points are displayed by squares for YM4-YFP and circles for RP437-YFP. (*A*) The half-height radius $r_{1/2}$ vs. c_0. The green dashed line marks the half-height radius $\sigma = 9.7$ μm of the fluorescein profile used to calibrate the serine profile. For both YM4-YFP and RP437-YFP, the swarm sizes are significantly larger than σ. (*B*) The contrast, defined as the ratio between the highest bacterial density in the swarm and the uniform bacterial density at infinity, $B_{max}/B_\infty \sim I_{max}/I_\infty$, was plotted against c_0. (*C*) The correlation *C* between the bacterial profile and the serine profile vs. c_0. This quantity is a measure of the bacterial nutrition uptake in a given attractant profile.

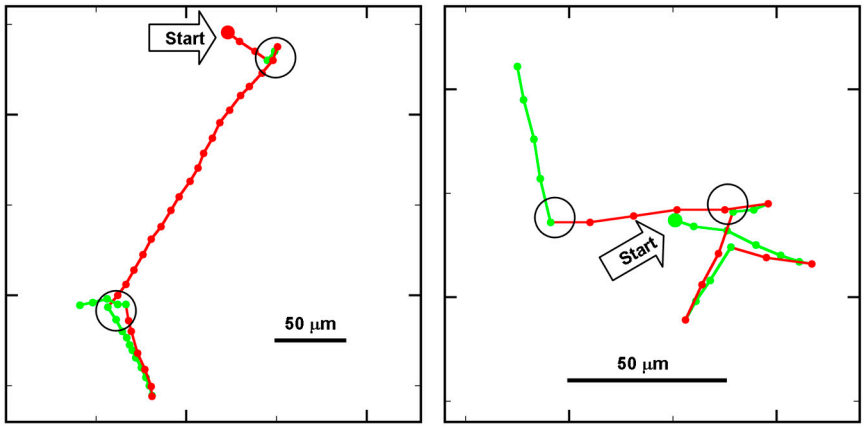

Fig. S7. Swimming trajectories of *P. haloplanktis* in seawater. The big solid circles are the starting points of the tracks. The green and red lines represent putative forward and backward swimming segments, respectively. These colors were assigned according to the three-step motility pattern of *V. alginolyticus*; i.e., a flick is always followed by forward swimming. The large open circles marked the flicking events, but not all flicks were marked for clarity. (Scale bar, 50 μm.)

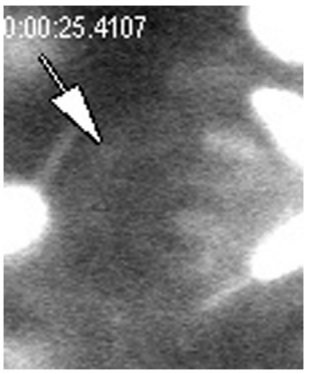

Movie S1. Bacterial swimming in TMN. This movie, along with Movie S2, illustrates how a bacterium uses its flagellum as a propeller and as a rudder. The bacteria were labeled with Nano Orange dye and viewed under the Nikon fluorescent microscope with a 100× objective. It is seen that the directional change (or a flick) occurs when a bacterium resumes its forward swimming. The arrows indicate the positions of the flagellum while flicking.
Movie S1 (AVI)

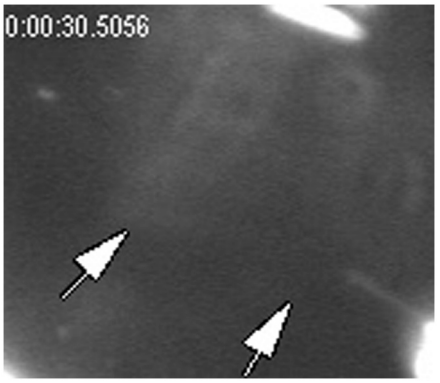

Movie S2. Bacterial swimming in TMN. This movie, along with Movie S1, illustrates how a bacterium uses its flagellum as a propeller and as a rudder. The bacteria were labeled with Nano Orange dye and viewed under the Nikon fluorescent microscope with a 100× objective. It is seen that the directional change (or a flick) occurs when a bacterium resumes its forward swimming. The arrows indicate the positions of the flagellum while flicking.
Movie S2 (AVI)

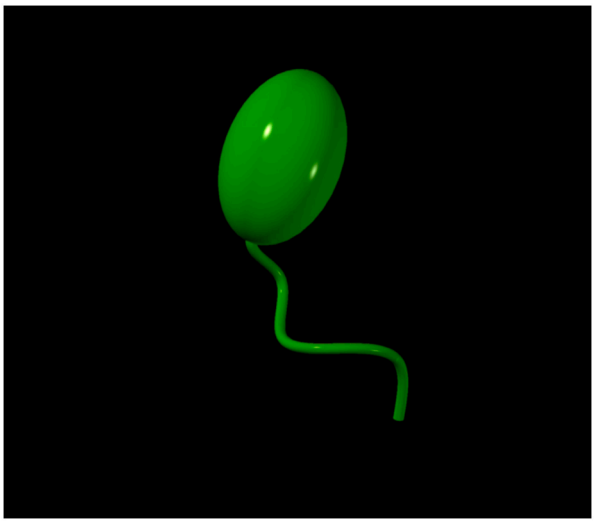

Movie S3. An animation of bacterial flagellar movement at the end of a flick. The bacterium changes its swimming direction by using the flagellum to push the cell-body at an angle (see both the main text and *SI Results and Discussion* for more detail). This animation schematically depicts how the flagellum realigns itself with the cell-body axis so that forward swimming can continue.
Movie S3 (WMV)

Table S1. Geometric parameters of *V. alginolyticus*

a, μm	b , μm	Ψ, °	L , μm	Λ, μm	R , nm	r , nm
0.4 (0.01)	1.8 (0.5)	36.2 (0.5)	4.59 (1)	1.49 (0.02)	140 (1)	16

The geometric parameters of *V. alginolyticus* given in this table are determined using fluorescence microscopy (1) and TEM (2). Here, a and b are the semiminor and semimajor axes of the cell-body; Λ, Ψ, L, and R are, respectively, the pitch, the pitch angle, the contour length, and the radius of the helical flagellum. The numbers in parentheses are standard errors of the means. The filament radius r was measured using TEM and its value is given in ref. 2

1 Chattopadhyay S, Wu XL (2009) The effect of long-range hydrodynamic interaction on the swimming of a single bacterium. *Biophys J* 96:2023–2028.
2 Magariyama Y, et al. (1995) Simultaneous measurement of bacterial flagellar rotation rate and swimming speed. *Biophys J* 69:2154–2162.